Article:
Chenchiliyan, M, Timpmann, K, Jalviste, E et al. (3 more authors) (2016) Dimerization of core complexes as an efficient strategy for energy trapping in Rhodobacter sphaeroides. Biochimica et Biophysica Acta - Bioenergetics, 1857 (6). pp. 634-642. ISSN 0006-3002

https://doi.org/10.1016/j.bbabio.2016.03.020

Dimerization of core complexes as an efficient strategy for energy trapping in Rhodobacter sphaeroides

Manoop Chenchiliyan[a], Kõu Timpmann[a], Erko Jalviste[a], Peter G. Adams[b], C. Neil Hunter[c], and Arvi Freiberg[a,d*]

[a]Institute of Physics, University of Tartu, W. Ostwald Str. 1, Tartu 50411, Estonia

[b]School of Physics and Astronomy, University of Leeds, Leeds, LS2 9JT, UK

[c]Department of Molecular Biology and Biotechnology, University of Sheffield, Sheffield S10 2TN, UK

[d]Institute of Molecular and Cell Biology, University of Tartu, Riia 23, Tartu 51010, Estonia

*__Corresponding author__: Tel: +37256453175, email:arvi.freiberg@ut.ee

Key words: Photosynthesis; light harvesting; photosynthetic excitons; LH1; LH2; RC.

Abstract

In the purple phototrophic bacterium Rhodobacter sphaeroides, light harvesting LH2 complexes transfer absorbed solar energy to RC-LH1-PufX core complexes, which are mainly found in the dimeric state. Many other purple phototrophs have monomeric core complexes and the basis for requiring dimeric cores is not fully established, so we analysed strains of Rba. sphaeroides that contain either native dimeric core complexes or altered monomeric cores harbouring a deletion of the first 12 residues from the N-terminus of PufX, which retains the PufX polypeptide but removes the major determinant of core complex dimerization. Membranes were purified from strains with dimeric or monomeric cores, and with either high or low levels of the LH2 complex. Samples were interrogated with absorption, steady-state fluorescence, and picosecond time-resolved fluorescence kinetic spectroscopies to reveal their light-harvesting and energy trapping properties. We find that under saturating excitation light intensity the photosynthetic membranes containing LH2 and monomeric core complexes have fluorescence lifetimes nearly twice that of membranes with LH2 plus dimeric core complexes. This trend of increased lifetime is maintained with RCs in the open state as well, and for two different levels of LH2 content. Thus, energy trapping is more efficient when photosynthetic membranes of Rba sphaeroides consist of RC-LH1-PufX dimers and LH2 complexes.

1. INTRODUCTION

Photosynthesis nourishes nearly all life on Earth either directly or indirectly. It begins with the absorption of solar energy by an antenna consisting of light harvesting (LH) protein complexes that contain highly organized and densely packed pigment chromophores. Excitation energy within the antenna eventually migrates to the reaction centre (RC), where a photochemical charge separation takes place [1-4]. Purple phototrophic bacteria such as Rhodobacter sphaeroides provide a valuable model for the study of energy trapping, due to their amenability to genetic manipulation, the availability of high-resolution structures of the major light-harvesting proteins, and detailed knowledge of the biogenesis and organisation of their photosynthetic membranes [5-13]. Whilst our understanding of this purple phototrophic bacterium is extensive there is still much we do not fully understand about the relationship between the LH complex organization and the energy transfer processes involved.

In most species of purple phototrophic bacteria, the photosynthetic membrane is composed of two types of closely packed arrays of LH complexes:(i) the 'core complex', comprised of light harvesting complex 1 (LH1) encircling the RC and (ii) the peripheral/distal light harvesting complex 2 (LH2) [3]. While the architecture of LH2 is relatively constant, the core complex design varies from species to species. The LH1 forms a closed ring or closed ellipse around the RC, for example, in Rhodospirillum (R.) rubrum, Rhodopseudomonas viridis, Rhodospirillum photometricum, and in Thermochromatium tepidum [7, 14-16], whereas some species of photosynthetic bacteria like Rhodobacter (Rba.) sphaeroides and Rhodopseudomonas (Rps.) palustris hold an additional polypeptide, PufX in Rba. sphaeroides and W in case of Rps. palustris, which creates a gap in the LH1 ring around the RC [17-19]. As reviewed in [20], the presence of PufX polypeptide in wild type Rba. sphaeroides leads most of the core complexes to assemble into S-shaped dimeric structures

[21-24], while a small percentage remains as closed-ring-shaped PufX-containing monomers [10].

Light-harvesting membranes from wild-type Rba. sphaeroides contain dimeric (LH1-RC-PufX)$_2$ core complexes organized into linear arrays, interconnected by LH2 complexes in vesicular membranes [8-10, 25-27]. The dimeric (RC-LH1-PufX)$_2$ core complex forms an S-shaped assembly of 28 LH1 subunits partially surrounding two RC, with a small gap in the LH1 structure at the RC Q_B site, provided by the positioning of PufX [21-23]. Deletion of the first 12 residues from the N-terminus of PufX removes the major determinant of core complex dimerization and results in monomeric core complexes containing PufX and 15 LH1 subunits [28]. A study comparing membrane organisation of wild-type, PufX-deletion and PufX-truncation mutants (with LH2) showed that monomeric core complexes still self-associate, but into clusters rather than the linear arrays found with dimeric core complexes [26, 28]. This also showed that the Rba. sphaeroides photosystem can be reconfigured to resemble that found in, for example, Rps. palustris [18]. From the above and [10], it is clear that the photosynthetic membrane of Rba. sphaeroides segregates into regions enriched in LH2, RC-LH1-PufX and cytochrome bc_1 complexes whereas other purple bacterial photosystems may have a more random organization [29, 30]. However, it is not known if these significant organizational differences confer any benefits in terms of energy trapping, a question we address in the current study. It appears that large LH2 antenna sizes, for example, do not improve trapping efficiencies to the expected extent; in a recent report [31] we studied the influence of the growth light-intensity on the efficiency of photosynthetic light harvesting in Rba. sphaeroides by measuring the rates of the delivery of excitation energy to the RCs and the quantum efficiency of charge separation in the low light and high light adapted membranes, which have high and low ratios of LH2/LH1, respectively. The trapping efficiency was found to decline in the samples with a high LH2/LH1 ratio. A complementary

result was reported by Driscoll et al. [32], who also proposed the presence of a considerable amount of disconnected LH2 complexes in the chromatophores of low-light adapted membranes.

The present study investigates the consequences of the PufX-mediated organisation of the bacterial photosystem in terms of the presence of RC-LH1-PufX dimers or RC-LH1-PufXΔ12 monomers influencing energy trapping properties. We analysed light-harvesting membranes in the form of 'chromatophores' (intracytoplasmic membrane vesicles) purified from strains of Rba. sphaeroides that contain either dimeric or monomeric core complexes together with controlled high or low LH2 contents. Samples were interrogated with absorption, steady-state fluorescence, and picosecond time-resolved fluorescence kinetic spectroscopies to reveal their light-harvesting properties. The study reveals the impact of the structural organization of the core complex on the energy transfer rates and the efficiency of trapping of antenna excitons. We conclude that energy trapping is more efficient when photosynthetic membranes of Rba sphaeroides consist of RC-LH1-PufX dimers and LH2 complexes.

2. MATERIALS AND METHODS

2.1 Samples

Purified chromatophores were prepared from cells grown under semi-aerobic conditions in an orbital shaker incubator, as described in [9]. By changing the degree of aeration of the culture, it is possible to control the LH2/LH1 ratio; a high degree of aeration produced a low LH2/LH1 ratio whereas a low degree of aeration formed a high LH2/LH1 ratio [33]. The strain used was DPF2G[pRKEH], which has the full complement of LH and RC complexes, but the LH2 genes are encoded on the genome whereas the RCLH1 and PufX genes are

encoded on a plasmid. DPF2G is a crtD variant of the DPF2 mutant described previously [28]; the crtD carotenoid background was used, since the core dimer/monomer ratio is high and the carotenoid composition is not influenced by the levels of aeration [34]. The second mutant strain DPF2G[pRKEHXΔ12] harbours a twelve-residue N-terminal truncation of PufX, giving core monomers that still have PufX [28]. These monomers represent one half of the RC-LH1-PufX core dimer, the structure of which was reported in [21, 22]. Biochemical data and atomic force microscopy data showed that the N-terminal truncation of PufX prevents dimerization of the core monomers [26, 28, 35], with 1 PufX and an estimated 15 LH1 subunits per monomer, as depicted in the insets in Fig. 1E, F. These two mutants were grown so they had either high or low LH2 levels, and for simplicity these chromatophore samples will be referred to as dimeric low LH2 (DL) and dimeric high LH2 (DH), and monomeric low LH2 (ML) and monomeric high LH2 (MH), according to their core structure (monomeric or dimeric) and the high or low levels of LH2 present.

The RC-LH1-PufX-only and LH2-only membranes, used in the present work for reference purposes (see Figs. 1 and 2), were prepared from the genetically modified mutant strains of Rba. sphaeroides, as described in [36].

All the samples were stored in freezer at -78°C until used. The defrosted concentrated samples were diluted before the experiments with the buffer solutions to obtain an optical density around 0.1 or 0.3 in the cuvette. The more concentrated samples were used in fluorescence lifetime measurements to provide a greater signal, as necessary. The chromatophore samples were diluted with 20 mM HEPES (pH 7.5) buffer solution mixed with 5 mM EDTA (ethylenediaminetetraacetic acid). The RC-LH1-PufX-only membranes were diluted with 10 mM HEPES (pH 7.5) mixed with 1 mM EDTA. The LH2-only membranes were diluted with 20 mM HEPES (pH 7.5). To mimic the fluorescence decay times typical of the active RC condition, the membranes were mixed with 5 mM sodium

ascorbate and 25 μM phenazinemethosulfate (PMS) along with the buffer solution (see [31] for the detailed effect of these chemicals).

2.2 Spectroscopy

As the spectroscopic setups applied in this study have been described recently [31], we shall give here only brief remarks.

The absorption spectra were measured using a commercial UV/VIS spectrophotometer (V-530, JASCO Corporation) with spectral resolution of 0.5 nm. In steady state fluorescence measurements the excitation was facilitated by a narrow-band (0.03 nm) Ti:sapphire laser (tuning range 675-1000 nm, 3900S, Spectra Physics) and the fluorescence was recorded through a spectrograph with the spectral resolution of 0.3 nm. In fluorescence kinetics measurements either a continuous wave mode-locked Ti:sapphire laser (tuning range 690-1000 nm, Coherent Mira-900) with the pulse repetition rate of 76 MHz, pulse duration of ~100 fs, and the excitation spectral band width of ~15 nm or a CW picosecond dye laser (tuning range 570-880 nm, Coherent 700, 76 MHz, 2-3 ps, ~5 nm) was applied. In spectrally dependent kinetic measurements, the fluorescence was recorded through a double subtractive dispersion monochromator (DTMc300, Bentham Ltd.) coupled to a streak camera (C1587, Hamamatsu). The spectral resolution of this instrumentation was 5 nm and the temporal resolution, determined as the full width at half maximum of the instrument response function, was 10 ps. In excitation intensity dependent measurements the fluorescence was recorded integrally, in the range from 875 nm to 925 nm using a set of band-pass filters and recoded either by a home-built synchroscan streak camera system with ~20 ps instrument response function [37, 38] (in lifetime measurements) or by Andor Technology DV420E-OE CCD camera (in fluorescence yield measurements). The use of two different kind of sample cells, a stationary cuvette and a rotating cell, enabled us to cover the several orders of magnitude excitation intensity span from active (all RCs open) to saturated (all RCs closed)

photosynthesis at reasonable signal to noise ratio. Like stirring, the rotating cell brings constantly into the excitable volume fresh portions of the sample with open RCs; thereby, by reducing the saturation, conditions for active photosynthesis are effectively achieved at higher average excitation intensity. The maximum output power of the excitation laser was successively attenuated by an appropriate combination of neutral density filters. All the measurements were performed at ambient temperature, 295±3K.

The measured fluorescence spectra as well as the decay curves were first appropriately corrected to the spectral and spatial sensitivity of the instruments and then fitted using the measured instrumental response function as described in [31]. Most of the decays were double-exponential. For those the weighted lifetime was evaluated as follows:

$$\tau_{av} = \frac{A_1\tau_1 + A_2\tau_2}{A_1 + A_2}, \quad (1)$$

where A_1, A_2, τ_1, and τ_2 are the amplitudes and decay times of individual decay components.

3. RESULTS

3.1 Evaluation of the LH2 to RC ratio from absorption spectra

In this work, we aimed to study the effect of core complex structure (dimeric vs. monomeric) on energy transfer efficiency, with all other variables comparable. Therefore, chromatophores were prepared from carefully chosen mutants and growth conditions, giving membranes that contained either dimeric or monomeric core complexes of similar LH2/LH1 content. Table 1 outlines the composition of the four basic mutant chromatophore samples studied herein.

Since it is not trivial to perfectly match the growth of different mutant cultures, a series of chromatophore samples were prepared at a high LH2/LH1 or low LH2/LH1 level (as described in the Materials and Methods section), and the best LH2/LH1 ratio-matched pairs

of the samples were chosen for subsequent detailed analysis. Absorption spectroscopy can be used to quantify the LH2/LH1 content, to confirm the suitability of the selected samples for a meaningful comparison.

Table 1. Composition of the samples tested in the current study.

Sample	Full mutant name	PufX	Core complex oligomerisation state
DL	DPF2G[pRKEH]	full length	Dimer: $(RC\text{-}LH1_{14}\text{-}X)_2$
ML	DPF2G[pRKEHXΔ12]	truncated	Monomer: $RC\text{-}LH1_{15}\text{-}X$ [e)]
DH	DPF2G[pRKEH]	full length	Dimer: $(RC\text{-}LH1_{14}\text{-}X)_2$
MH	DPF2G[pRKEHXΔ12]	truncated	Monomer: $RC\text{-}LH1_{15}\text{-}X$ [e)]

[e)] The number of LH1 subunits is estimated to be 15 based on biochemical and AFM data showing monomeric core complexes [26, 28] and comparison to the known structure of monomeric RC-LH1-PufW from Rps. palustris [19].

Figure 1 shows the absorption spectra in the near-infrared range of selected four samples corresponding to low and high LH2 content dimeric and monomeric samples. All the spectra are composed of three strong absorption bands at about 800 nm, 850 nm, and 875 nm. The two former peaks, commonly referred as B800 and B850 are related to the LH2 peripheral complex, while the latter, B875, to the LH1 core complex [39-41]. The generally well-overlapping spectra (panels A and B) of the samples with dimeric and monomeric core complexes indicate that the selected samples have similar LH2/LH1 ratio. The enlarged intensity variations observed in the B800 absorption range are common for the membrane samples, but as yet not well understood.

In order to more accurately quantify the LH2/LH1 content, we deconvoluted the measured absorption spectra into LH2 and LH1 constituent bands like in [31, 42].

As illustrated in Fig. 1, panels C to F, the absorption spectra of the samples were fitted in the wavelength range from 700 nm to 950 nm to the sum of the separately measured absorption spectra of the mutant membranes that contain either only the LH2 or dimeric RC-

LH1-PufX complexes (the latter sample is hereafter termed D-only). The 850 nm band of LH2 was fitted more carefully than the 800 nm band owing to the inherent intensity variations in the B800 absorption band. The constituent spectra were also allowed to shift slightly in wavelength scale to attain their linear combination of closest match to the measured spectrum. No shift was actually needed in case of DH and ML samples, while the maximum required shift of the fitting sub-spectra for DL and MH samples was 1 nm, respectively, towards the red end and blue end of the spectrum.

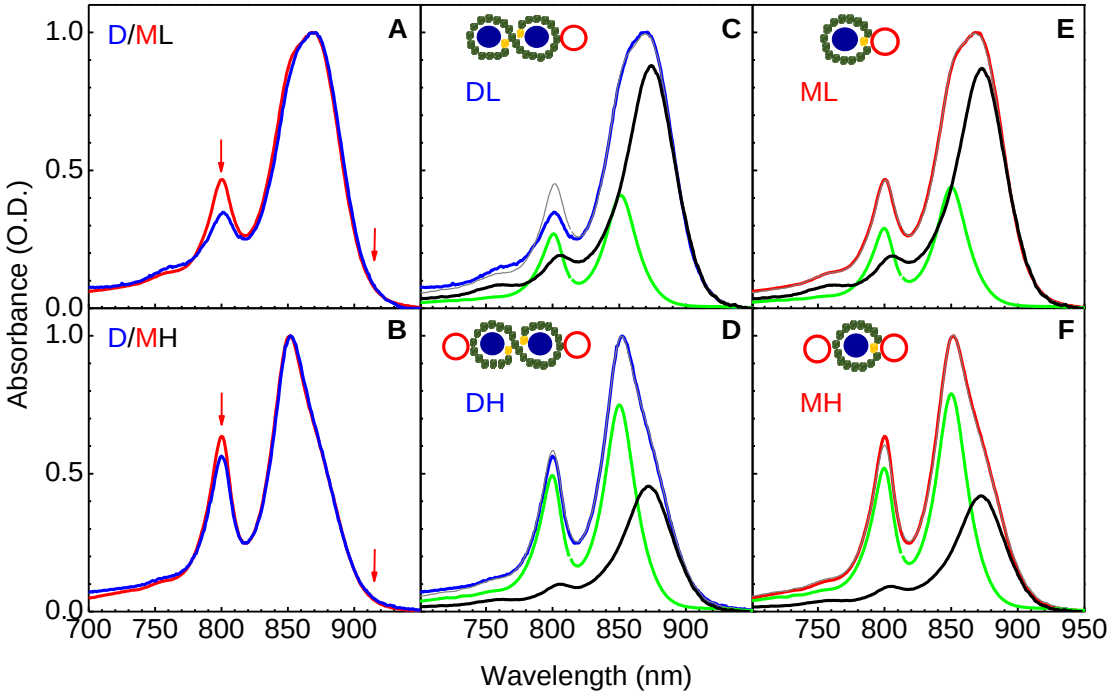

Fig. 1. (A, B) Comparison of the absorption spectra of membranes from Rba. sphaeroides strains containing monomeric (red) or dimeric (blue) core complexes, and with low (A, C, E) or high (B, D, F) content of LH2. The red arrows indicate the selective excitations used in stationary fluorescence measurements described in section 3.2. (C-F) Decomposition of the spectra for the same samples. The sub-spectra of the LH2-only and D-only membranes used in the fit are coloured in green and black, respectively. The measured curves are shown in red (monomeric) or blue (dimeric) and the simulated curves in grey. Each inset in panels C-F illustrates the composition of samples. Two (one) red rings indicate high (low) relative LH2 content, respectively, each green dot represents the bacteriochlorophyll-a (BChl) αβ-$BChl_2$ heterodimer subunit of the LH1 core complex, a light yellow dot represents PufX polypeptide and a blue circle represents RC.

The integrals, i.e. the areas below the fitted curves, of the component spectra in the range from 700 nm to 950 nm were then used to evaluate the ratio of peripheral and core complexes, LH2/LH1. Assuming equal absorption of the bacteriochlorophyll-a (BChl) chromophores in LH2, LH1 complexes as well as in RC's and knowing the number of BChls in LH2 (27 [43]), RC-LH1-PufX dimer (56 in LH1 and 4×2 in RC [7, 42]), and RC-LH1-PufX monomer (30 in LH1 and 4 in RC [20]), the LH2/LH1 ratio was evaluated. Finally, taking into account the number of RCs per core complex (2 for dimeric, 1 for monomeric case) the calculated LH2/RC ratio was obtained, as presented in Table 2.

Table 2. Ratio of the LH2 to RC complexes (±5%) in Rba. sphaeroides strains with LH2 and core monomers or dimers.

Sample	B875/B850 integral absorbance ratio	Calculated LH2/RC ratio
DL	0.42	0.50
ML	0.46	0.58
DH	1.51	1.79
MH	1.60	2.02

The low-LH2 matched samples (DL vs. ML) have ~14% difference between LH2/RC ratios and high-LH2 matched samples (DH vs. MH) ~12% difference. This confirms that our dimeric and monomeric samples are sufficiently well matched that we can proceed with analysis of energy transfer by fluorescence spectroscopy described in the following sections.

3.2 Relative yield of the LH2 and LH1 fluorescence as a function of the LH2 to RC ratio and the excitation wavelength

This section explores the steady-state fluorescence spectra of the monomer-dimer core samples shown in Fig. 2. Selective excitation was provided predominantly into either the peripheral LH2 antenna at 800 nm or core LH1 antenna at 915 nm, as indicated by the arrows on the absorption spectra in Fig. 1 A and B. The excitation intensities used correspond to the

saturated photosynthesis where most of the RCs are inactive/closed. If the B800 BChls are excited with the 800 nm light, the photoinduced exciton can transfer energetically 'downhill' along the ladder of different intermediate states: B800 (LH2) -> B850 (LH2) -> B875 (LH1) -> RC. During each stage part of the excitation energy is lost as fluorescence until the exciton is eventually 'captured' by photochemistry at the RC. The fluorescence emission from B800 and RC BChls is suppressed owing to their short lifetimes [44-46]. Therefore, the observed fluorescence mostly originates from the B850 (LH2) and B875 (LH1) BChls. Hereafter, these dominant fluorescence components are denoted by F850 and F875 corresponding to the LH2 emission maximum at ~860 nm and LH1 emission maximum at ~890 nm, respectively (see inset of Fig. 2A).

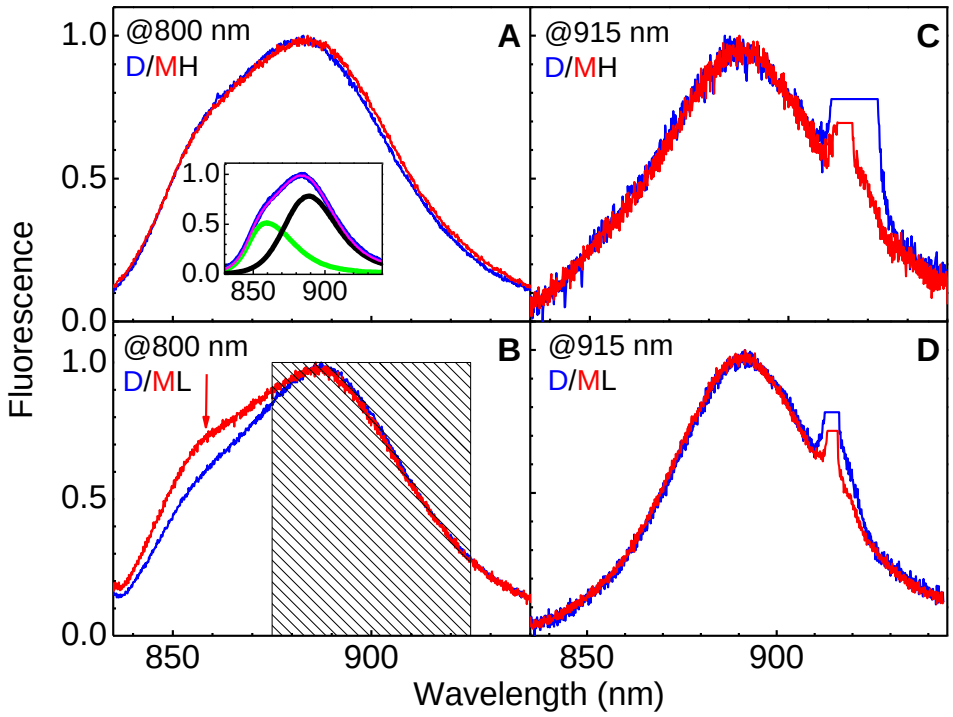

Fig. 2. Normalized fluorescence spectra of the samples with dimeric or monomeric LH1 core and with high (A, C) or low (B, D) LH2 content following excitation at 800 nm (A, B) or at 915 nm (C, D). The samples with dimeric core are shown by blue curves and those with monomeric core, by red curves. All the spectra are measured at saturated state of photosynthesis. The inset of panel A shows the deconvolution of the DH fluorescence spectrum (blue) at 800-nm excitation into the F850 (green curve) and F875 (black curve) constituents. The component spectra used in the fit are measured spectra of LH2-only sample

and D-only sample. The sum of the components (narrow magenta line) is practically overlapping with the measured spectrum. The red arrow highlights the extra LH2 fluorescence emission observed in the ML sample. A scattered excitation light artefact in panels C and D is evident at 915 nm. Hatched area in panel B indicates the spectral range of the band pass filter used in the intensity dependent kinetic measurements (Section 3.3).

By monitoring the relative level of emission, F850 or F875, information can be obtained on the fate of excitons dependent on where they originate. For example, one may expect, in qualitative agreement with Fig. 2 A and B, that with 800-nm excitation high proportion of LH2s in the sample will be excited, which would result in a prominent F850 contribution. Selective excitation into the B875 band at 915 nm, instead, should lead to a broad F875 emission and very little if any F850 emission. Close look on Fig. 2 C and D reveals that with 915-nm excitation there indeed is a measurable contribution of the F850 fluorescence that increases with the LH2/RC ratio (see Fig. 3). Neglecting any possibility of direct excitation of LH2, the F850 emission may be generated by energetically "up-hill" excitation transfer from LH1 to LH2, brought into effect by high (physiological) temperature [47-50].

Regardless of the difference in structural organization, the observed fluorescence spectra following 915-nm excitation of monomeric and dimeric core complexes match each other well both at low and high LH2 concentration (Fig. 2 C and D). At 800 nm excitation, the spectra of high LH2-content samples also appear to be relatively well matched (Fig. 2A), whereas the low LH2 samples in the presence of monomers show much enhanced LH2 emission, highlighted by an arrow in Fig. 2 B. This issue will be further discussed below.

Figure 3 displays the ratio of the integrated fluorescence intensities (or fluorescence yields) of the LH2 and LH1 sub-bands, F850/F875, as a function of the LH2 content relative to RC. Relative contributions of the F850 and F875 components were obtained by

deconvoluting the stationary fluorescence spectra of interest as illustrated in the inset of Fig. 2A. [31]. These deconvolutions were performed using the energy scale.

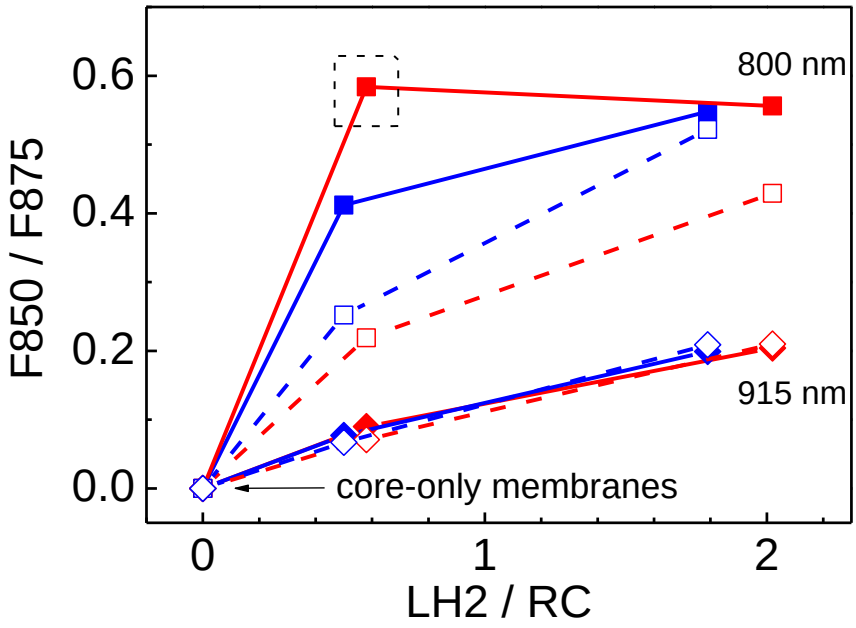

Fig. 3. Dependence of the fluorescence yield, F850/F875, on the LH2 to RC ratio upon 800 nm (squares) and 915 nm (rhombi) excitations. The data for dimeric and monomeric core samples are distinguished by blue and red colours, respectively. The lines connecting these data points are for guiding the eye. The correspondingly coloured dashed lines with un-filled data points display the calculated fluorescence yield ratios, as described in Section 4.1. The dashed rectangular outlines the data point most drastically deviating from modelling result. The data at LH2/RC = 0 correspond to the samples comprising solely core complexes.

In Fig. 3, there is a general trend of increasing F850/F875 ratios with LH2/RC. Furthermore, the F850/F875 ratio following 800-nm excitation is always greater than that at 915-nm excitation. These tendencies appear logical because both direct excitation of LH2 and higher LH2 content favour the contribution of F850. However, in low LH2 samples at 800 nm excitation, the experimental F850/F875 ratios are way larger than the calculated ones, according to the model that will be introduced in Section 4.1. For the reasons clarified below, current samples also show greater F850/F875 ratios under 800 nm excitation than the previously studied wild-type chromatophores at similar LH2/RC ratios [31].

3.3 Excitation intensity dependent fluorescence yield and decay time

The above contradictions highlight the need to complement steady state emission spectra with time-resolved measurements. Since both kinetic and steady state emission parameters of photosynthetic bacteria depend on the state of their RC (open or closed), this state being a function of the excitation intensity [38, 51], we will first examine the excitation intensity dependence of the fluorescence lifetime and the fluorescence yield. The fluorescence was recorded between 875 and 925 nm, the spectral range of dominant LH1 emission, as shown in Fig. 2B. The fluorescence yield data points were evaluated by dividing the obtained integrated intensity with the excitation intensity. Note that the absorbed power is presumed to be proportional to excitation intensity.

The results of such measurements, which show generic increase with excitation light intensity of the fluorescence yield and lifetime, are demonstrated in Fig. 4. As excess excitation intensity is known to lead to a non-linear excitation quenching [31, 51-55], we limited our data analysis to the excitation intensities below $5*10^{-2}$ W/cm^2. The fluorescence lifetime corresponding to the active photosynthesis plateau evident in fluorescence yield measurements could only be achieved by adding reducing agents PMS and ascorbate to the sample, which maintain the RCs in open state. According to Clayton et al. [56], these reducing agents collectively prevent the accumulation of P+ states at high excitation intensity. As shown in our previous publication [31], data on samples with PMS and ascorbate generally match the low-intensity plateau for the yield and lifetime, irrespective the applied excitation intensity. We consequently assume that in current experiments the open RC state corresponds to a reduced BChl special pair (customarily designated as P), while the closed RC state to an oxidized special pair (P+).

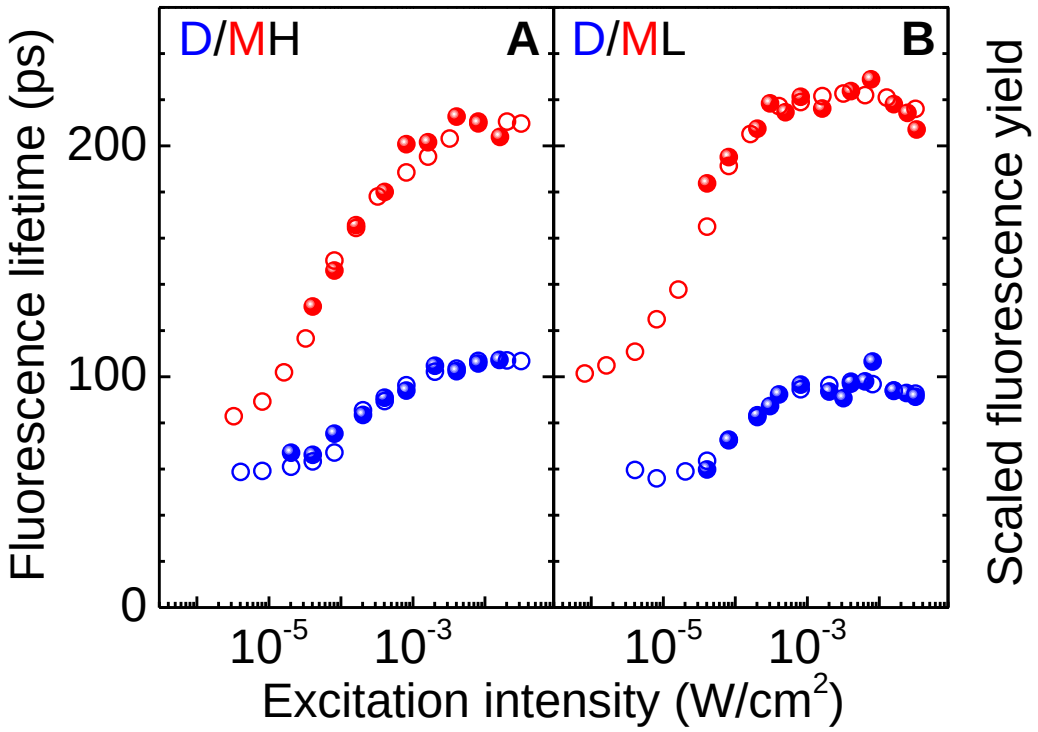

Fig. 4. Excitation intensity dependence of the dominant short fluorescence lifetime component (filled spheres, left Y-axis) and the fluorescence yield (open circles, right Y-axis). The data for dimeric and monomeric core samples are distinguished by blue and red colours, respectively. Panels A and B, correspondingly, present data of high and low LH2 content samples. The yield data are scaled until matching with lifetime values in order to visualize the proportionality of these quantities. The increase in lifetime and yield corresponds to the transition from the open to the closed RC state. The samples from Rba. sphaeroides were excited at 590 nm for the decay kinetics and at 800 nm for the stationary fluorescence yield measurements.

Similar dependences on the excitation intensity that clearly distinguish the active (corresponding to the low excitation intensity plateau) and the saturated (the high intensity plateau) stages of photosynthesis were observed in wild-type membranes of Rba. sphaeroides [31]. However, in Fig. 4 we notice that samples containing monomeric cores (ML and MH) hold distinctively higher fluorescence lifetimes than samples with dimeric cores (DL and DH) at all excitation intensities. Relative differences between the samples with high and low LH2 content (MH vs. ML or DH vs. DL) appear to be much less significant.

Table 3 displays the fluorescence lifetimes for the studied sample set corresponding to active and saturated photosynthesis states. Although the data were generally fitted assuming double-exponential decay kinetics, as the contribution of the second, long component (~ 430 ps) was typically rather small (< 5%), only the values of the shorter lifetime are presented here. The special case of the DL sample, where the contribution of the long component was significant (~30%) at saturated photosynthesis, will be discussed separately.

Table 3. The dominant short fluorescence lifetime component (±10%) in picoseconds corresponding to active (noted by superscript o) and saturated (superscript c) ranges of photosynthesis with, respectively, mostly open and mostly closed RCs.

Samples	**Active (τ^o)**	**Saturated (τ^c)**
DL	42	97
ML	56	221
DH	44	103
MH	59	206

Comparison of lifetimes in Table 3 confirms the qualitative conclusion made by observation of Fig. 4 that samples with monomeric cores have a consistently longer fluorescence lifetime than those of dimeric cores, irrespective of their LH2 content or the RC state (open or closed). The difference between monomers and dimers is most prominent in case of closed RCs (τ^c(ML)/ τ^c(DL)=2.28 and τ^c(MH)/ τ^c(DH)=2.00), but is still significant with open RCs (τ^o(ML)/ τ^o(DL)=1.33 and τ^o(MH)/ τ^o(MH)=1.34). On the other hand, the lifetimes are very similar between low/high LH2 content with the same type of core complex (the ratios range between 0.94 and 1.07). Assuming identical hopping time for an exciton created in the distal LH2 antenna migrating towards the core complex in monomeric and dimeric strains with similar LH2 antenna sizes, the observed difference in the exciton quenching time by open and closed RCs can be assigned to the effects of the monomer/dimer

status of core complexes on the structural organization of the photosynthetic membrane. This issue will be addressed further in Discussion section.

Since the LH2->LH1 energy transfer features are most clearly revealed in the kinetics of the B850 emission around 820-870 nm [32], spectrally resolved emission kinetics upon 800 nm excitation were measured with 5 nm spectral resolution in the range from 820 to 920 nm covered by 10 nm wavelength step. The kinetic traces were fit using two or three exponential components in the case of closed or open RC state, respectively. For brevity, in Table 4 we present only the most representative results of these measurements, namely the averaged over few data points lifetime of the dominant fluorescence component at the blue end (<850 nm) and the red end (≥880 nm) of the observed spectrum. The data points corresponding to active photosynthesis are measured using the samples with chemically reduced RCs. The blue-end lifetime we assign to the LH2 to LH1 excitation transfer, and the red-end lifetime to the trapping in case of open RCs or to the quenching in case of closed RCs. The active and saturated case red-end lifetimes in Table 4 are in excellent agreement with those from Table 3 that represent the average lifetime of spectral components passing through 875-925 nm band pass filter.

Table 4. The lifetime in picoseconds of the dominant short component of the fluorescence decay (±10%) at blue and red ends of the fluorescence spectrum in case of active and saturated photosynthesis.

Samples	**Active (τ^o)**		**Saturated (τ^c)**	
	Blue end (≤850 nm)	Red end (≥880 nm)	Blue end (≤850 nm)	Red end (≥880 nm)
DL	27	42	29	97
ML	37	56	35	216
DH	24	44	25	108
MH	25	59	33	205

4. DISCUSSION

The major experimental revelation of this work has been that under saturating light intensity the photosynthetic membranes containing LH2 and monomeric core complexes appear to have fluorescence lifetimes nearly double that of LH2 plus dimeric core complexes (Fig. 4, Tables 3 and 4). This trend of increased lifetime is maintained also with the RCs in the open states, and for two different levels of LH2 content. To comprehend these observations, kinetic modelling of the rate constants was performed as follows. The analysis reveals differences in the excitation energy transfer dynamics in LH membranes according to the structure of the core complex.

4.1 Kinetic model and evaluation of microscopic rate constants

A kinetic model adopted here and shown in Fig. 5 is similar to the one used in our previous work [31]. It defines a mathematical relation between the 'apparent' rate constants, γ, each characterizing an exponential component of the observed multi-exponential fluorescence decay, and the 'microscopic' rate constants, k, each characterizing a specific kinetic pathway. According to this basic model (right part of Fig. 5), the apparent rate constants γ_1 (the inverse of the lifetimes presented in Table 4 measured at ≤850 nm) and γ_2 (the inverse of lifetimes in Table 4 at ≥880 nm), and the microscopic rate constants are connected as follows [47]:

$$\gamma_1 = \frac{1}{2}\left[\left({k_{loss}}^{LH2} + k_1 + k_{-1} + {k_2}^{o,c}\right) + \sqrt{\left({k_{loss}}^{LH2} + k_1 - k_{-1} - {k_2}^{o,c}\right)^2 + 4k_1k_{-1}}\right]$$

$$\gamma_2 = \frac{1}{2}\left[\left({k_{loss}}^{LH2} + k_1 + k_{-1} + {k_2}^{o,c}\right) - \sqrt{\left({k_{loss}}^{LH2} + k_1 - k_{-1} - {k_2}^{o,c}\right)^2 + 4k_1k_{-1}}\right] \quad (2)$$

In Eq. 2, k_1 and k_{-1} are, respectively, the forward and backward energy transfer rate constants between the LH2 and LH1 compartments; ${k_{loss}}^{LH2}$ is the total rate constant of the excitation loss from the LH2 compartment apart from the transfer of excitation energy to

LH1, and $k_2^{o,c}$, the decay rate constants of LH1 excitons in case of open (k_2^o) and closed (k_2^c) RCs. For convenience, we have also defined that $k_2^{o,c}$ is a sum of the trapping rate constants, $k_t^{o,c}$, by open or closed RCs, and k_{loss}^{LH1}, the rate constant of any other kind of decay of LH1 excitons apart from their transfer to RC, i.e.:

$$k_2^{o,c} = k_t^{o,c} + k_{loss}^{LH1}. \quad (3)$$

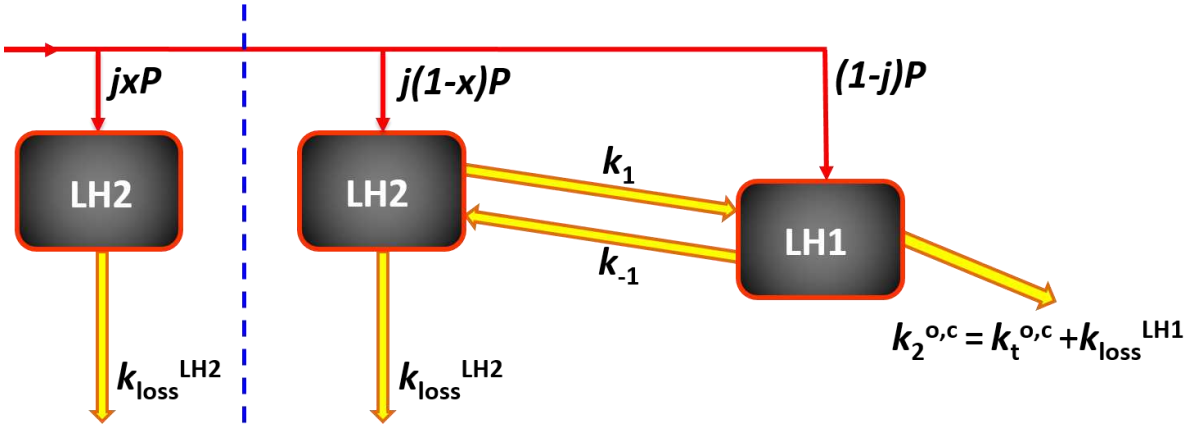

Fig. 5. Kinetic scheme of exciton population dynamics of the photosynthetic unit of purple bacteria. The basic scheme (right from the vertical dotted demarcation line) comprises functionally connected LH2 and LH1 compartments. An additional compartment used in the extended model represents functionally unconnected or poorly connected LH2 pool. The total absorbed power is denoted by P. Red arrows illustrate the branching of the absorbed power between the compartments governed by the factors j and x, where $0 \leq j,x \leq 1$. The factor x represents a fraction of unconnected LH2 units. Each kinetic pathway is characterized by a rate constant.

The k_{loss}^{LH1} values for membranes containing PufX or PufXΔ12 core complexes, but devoid of RCs, are not available. However, it is reasonable to assume that they are similar to the reciprocal of the fluorescence decay time of the ring-shape mutant LH1-only membrane of Rba. sphaeroides (1/450 ps^{-1}, determined in [31]). We presume that $k_2^{o,c}$ does not change with the LH2 to RC ratio, i.e. $k_2^{o,c}(DL) = k_2^{o,c}(DH)$ and $k_2^{o,c}(ML) = k_2^{o,c}(MH)$. Under thermal equilibrium, the forward (LH2 -> LH1) and backward (LH1-> LH2) energy transfer rates, k_1 and k_{-1} (assumed to be independent from the RC state) are related to each other via the Boltzmann factor. The equilibrium constants, $K = k_1 / k_{-1}$, in all studied samples were

calculated according to the equation presented in [31, 47]. The decay rate of the exciton in the LH2-only membrane, $k_{loss}{}^{LH2}$, is around 1/500 ps^{-1} [31].

For given values of microscopic rate constants and the branching ratio the steady-state fluorescence yield ratio, F850/F875, can be calculated by [31, 47]

$$\frac{F_{850}}{F_{875}} = \frac{k_{-1} + jk_2}{k_1 + k_{loss}{}^{LH2}(1-j)} \quad . \tag{4}$$

In Eq. (4), j and (1–j) describe the branching of the excitation between the LH2 and LH1 compartments, respectively. As can be seen in Fig. 1, at 800 nm excitation, a branching of the absorbed photons between the LH2 and LH1 pools takes place due to overlap of their absorption spectra. The values of the branching ratio, j, for 800 nm excitation for all the samples were determined from the absorption spectra shown on Fig. 1 as in [31]. An effect of excitation de-trapping from RC [57-60] on the LH2/LH1 branching ratio is small [31] and has been ignored here. LH1 is then the only complex that absorbs under 915 nm excitation, i.e. we assume j = 0 in this case.

Considering the above prerequisites and applying Eqs. 2-4, all the relevant microscopic rate constants as listed in Table 5 were determined iteratively to harmonize the calculated and experimental fluorescence yields and lifetimes. A distinctive feature of the numbers in Table 5 is that $1/k_2$, the decay time of LH1 excitons, is reproducibly longer in case of monomeric core complexes compared with dimeric ones. It is also evident that relative difference of the $1/k_2$ times between monomeric and dimeric samples increases upon closing RCs.

The data shown in four last columns of Table 5 satisfactorily reproduce corresponding experimental lifetimes presented in Table 4. This seems to verify the model and its predictions. However, agreement between the calculated and measured relative fluorescence yields, F850/F875, is limited. At low LH2/RC ratio and 800-nm excitation, the samples show

significantly larger F850/F875 than predicted by the model, with the least satisfactory fit observed for the ML sample (see Fig. 3). Note that according to the model, the F850/F875 ratio in dimeric core samples is always larger than in monomeric core samples. This is because of relatively shorter lifetime of the B875 excitons compared with B850 excitons in dimeric samples.

Table 5. The calculated microscopic forward energy transfer time, ${k_1}^{-1}$, backward energy transfer time, ${k_{-1}}^{-1}$, quenching time either by open RC, ${k_2}^{o^{-1}}$, or by closed RC, ${k_2}^{c^{-1}}$, apparent LH2->LH1energy transfer time in case of open (closed) RC, $\gamma_1^{o^{-1}}$ ($\gamma_1^{c^{-1}}$), and apparent trapping time, $\gamma_2^{o^{-1}}$, and apparent quenching time, $\gamma_2^{c^{-1}}$. All the calculated times have an uncertainty up to 10% of their numerical value.

Sample	$\frac{1}{k_1}$ **(ps)**	$\frac{1}{k_{-1}}$ **(ps)**	$\frac{1}{{k_2}^o}$ **(ps)**	$\frac{1}{{k_2}^c}$ **(ps)**	$\frac{1}{\gamma_1^o}$ **(ps)**	$\frac{1}{\gamma_1^c}$ **(ps)**	$\frac{1}{\gamma_2^o}$ **(ps)**	$\frac{1}{\gamma_2^c}$**(ps)**
DL	30	420	30	93	23	26	38	100
ML	38	494	45	185	30	33	54	195
DH	32	144	30	93	19	24	46	113
MH	42	185	45	185	27	32	65	211

Critical analysis of the fluorescence yield data lead us to a conclusion that the observed irregularities are likely related to contamination of the samples by some functionally disconnected or poorly connected LH2 complexes, which artificially amplify the F850/F875 value. Indeed, our samples may contain certain amount of the biosynthetic precursor membrane [33] (also termed the upper pigmented band from its position in sucrose gradients), formed in early stages of membrane maturation. Due to some disconnected LH2 complexes in the upper pigmented band, energy transfer is less efficient from LH2 to LH1 in comparison with matured intracytoplasmic membranes [9, 27, 61]. In wild-type strains the precursor and mature chromatophore membranes are usually well separated in sucrose density gradients [12] but the separation is less effective in mutants with monomer cores, when LH2 levels are low [26].

To evaluate relative fraction of disconnected or poorly connected LH2s, we extended the basic kinetic model by adding the left part of Fig. 5. The relative share of functionally disconnected LH2s for all studied samples were estimated according to Eq. (A9) in [31]. To achieve consistency with experimental data, the calculated relative fraction of functionally disconnected LH2s is <5% in all samples, except the ML sample, where their contribution reaches ~ 16%.

4.2 Quantum efficiency of energy trapping

A highly significant finding of this study is the shorter LH1 excited state lifetime observed in membranes containing dimeric core complexes compared with monomeric ones. We propose that the shorter lifetime for dimeric complexes is due to excitation sharing across a larger LH1 antenna with access to two traps, i.e. the presence of two RCs instead of one per LH1 assembly, resulting in increased trapping or quenching probability of LH1 excitons at low or high excitation intensity, respectively. Comayras et al [61] previously showed that such excitation sharing occurs; the current study explains how this may improve the efficiency of the complex. This notion is confirmed by separate fluorescence kinetics and yield measurements on isolated dimeric and monomeric core complexes (work in progress, data not shown). Another effect that may contribute into the varying lifetime between the membranes containing monomeric or dimeric cores may arise from core monomers reorganising the photosynthetic membrane, as shown in a previous study [26]. In the AFM topographs recorded in [26], the tendency of core dimers to form short linear arrays and LH2 to form large LH2-only assemblies was changed and a more random arrangement was seen, consisting of core monomers interspersed among LH2 complexes. Better structural connectivity in LH1 and RC pools for the dimeric core complexes implies larger LH1 to LH1 and RC to RC excitation transfer rates that may lead to increased probability for the excitation to reach an open RC in the same or in neighbouring core complexes if the RC of a

given core is in a closed state [62]. Advanced computational modelling, as performed for wild-type membranes [10, 42, 63-66], would certainly be helpful for a deeper analysis of energy trapping in core monomer and core dimer membranes.

We will next consider how the core complex structure and the excitation wavelength affect the quantum efficiency of active (all RCs in open state) photosynthesis. The equation for quantum efficiency,

$$\eta = \left(k_2^o - {k_{loss}}^{LH1}\right)\left(\frac{1+{k_{loss}}^{LH2}(1-\mathrm{j})/\mathrm{k_1}}{k_2^0+{k_{loss}}^{LH2}\left(1/K+k_2^0/\mathrm{k_1}\right)}\right) \quad , \tag{5}$$

was taken from [31]. The efficiencies calculated by Eq. (5) using the microscopic rate constants from Table 5 are presented in Fig. 6. The efficiencies for solely core complexes (case LH2/RC=0) were calculated according to modified Eq. (5), $\eta = \left(k_2^o - {k_{loss}}^{LH1}\right)/\, k_2^0$, using the same rate constants as for other samples. All the efficiencies have a standard deviation of ~2% of the calculated values, indicated by the shaded area in Fig. 6. The major factors that contribute into the error estimate are (i) uncertainty in determining the experimental fluorescence lifetimes; (ii) uncertainty in evaluating the excitation branching factor, j; (iii) possible flexibility in finding the model rate constants.

According to Fig. 6, quantum efficiency of energy trapping is consistently found higher in samples with dimeric core. The efficiency generally decreases with increasing LH2/RC ratio, concurrent with computational modelling studies where efficiency of energy transfer across the entire chromatophore was simulated [10, 42, 65]. Furthermore, both in monomeric and dimeric samples, the absolute efficiency is always higher at 915-nm excitation compared with 800-nm excitation, unless the limiting case of LH2/RC=0 when they are expected to overlap. Qualitatively similar behaviour was observed in our previous study of wild-type membranes [31].

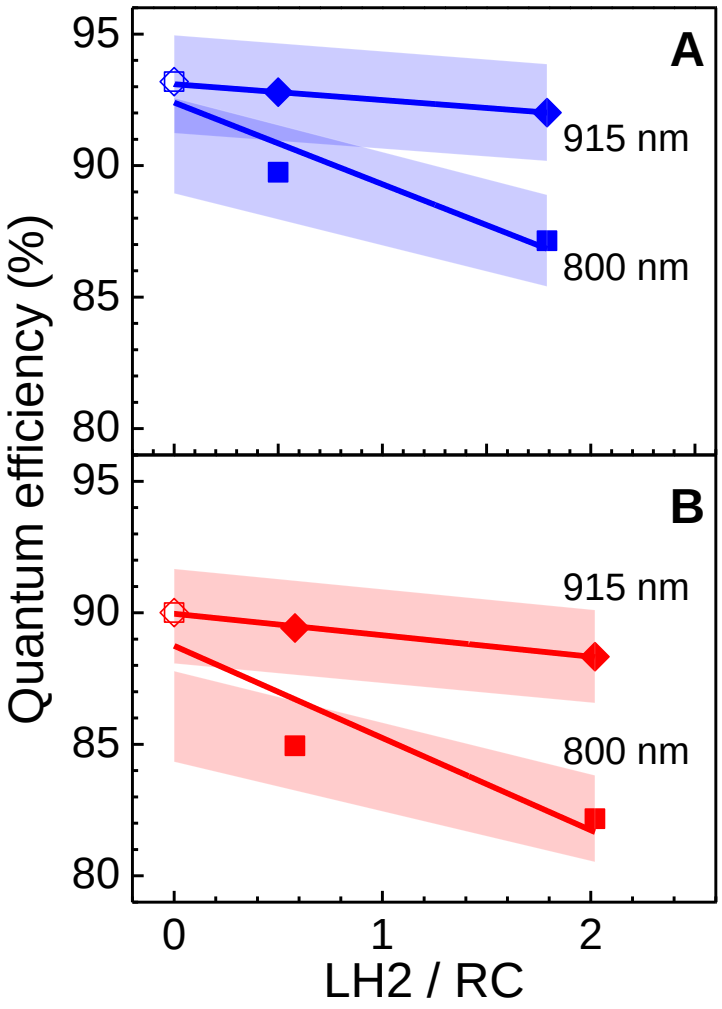

Fig. 6. The dependence of quantum efficiency of active photosynthesis on the LH2 to RC ratio in dimeric (A) and monomeric (B) core samples upon 800 (squares) and 915 nm (rhombi) excitation. The open data points at LH2/RC=0 correspond to the quantum efficiencies of the imaginary membranes containing either sole dimeric or sole monomeric core complexes. The shaded area features the ~2% estimated standard deviation in the efficiency. The lines represent linear fits of the data points. See text for further explanations.

At 915-nm excitation, LH1 is directly excited and the exciton does not have to travel between multiple different LH complexes. At 800 nm the excitation probes the longer LH2->LH1->RC pathway involving LH2, compared to only LH1->RC transfer with 915 nm excitation. Thus, any difference between the efficiencies under 800- and 915-nm excitation at LH2/RC≠0 informs us about the LH2->LH1 transfer. Conversely, quantum efficiency of the mutant membranes lacking LH2 complexes should be the same, irrespective the excitation

wavelength. Linear fits of the data points in Fig. 6 show that within the experimental uncertainty the efficiencies at 800- and 915-nm excitation indeed converge. The convergence is relatively poorer in case of monomeric core samples upon 800-nm excitation due to the above presence of functionally disconnected or poorly connected LH2 units in these samples.

5 Conclusions

In this study we provide a thorough comparison of the fluorescence properties of Rba. sphaeroides chromatophores containing LH2 and either monomeric or dimeric core complexes, which reveals differences in their energy transfer and trapping properties. The exciton quenching time by open and closed RCs in the LH membranes with LH2 and monomeric core complexes was always found to be significantly longer compared to the samples with dimeric core, irrespective of the excitation wavelength or the LH2 to RC ratio. As a result, the quantum efficiency of photon energy trapping was concomitantly higher in LH membranes with dimeric cores. In summary, we clearly show that it is advantageous to have dimeric core complexes as recipients for energy harvested by LH2 complexes in Rba. sphaeroides.

Acknowledgements

This work was supported by the Estonian Research Council (grant IUT02-28), the ESF DoRa 4 program (grant NLOFY12523T), and the H2020-MSCA-RISE-2015 program (grant 690853). CNH gratefully acknowledges financial support from the Biotechnology and Biological Sciences Research Council (BBSRC UK), award number BB/G021546/1. CNH was also supported by an Advanced Award 338895 from the European Research Council and as part of the Photosynthetic Antenna Research Center (PARC), an Energy Frontier Research Center funded by the U.S. Department of Energy, Office of Science, Office of Basic Energy Sciences under Award Number DE-SC 0001035. PGA was supported by a doctoral studentship and an Anniversary Future Leader Fellowship from the Biotechnology and

Biological Sciences Research Council (UK). We are grateful to Girinath G. Pillai for generating the graphical representation of RC-LH1-PufX dimer complex from Rba. sphaeroides.

References

[1] R.v. Grondelle, J.P. Dekker, T. Gillbro, V. Sundstrom, Energy transfer and trapping in photosynthesis, Biochim. Biophys. Acta, 1187 (1994) 1-65.
[2] A. Freiberg, Coupling of antennas to reaction centers, in: R.E. Blankenship, M.T. Madigan, C.E. Bauer (Eds.) Anoxygenic Photosynthetic Bacteria, Kluwer Academic Publishers, Dordrecht, The Netherlands, 1995, pp. 385-398.
[3] R.E. Blankenship, Molecular Mechanisms of Photosynthesis, Blackwell Science, Oxford, United Kingdom, 2002.
[4] R.J. Cogdell, A. Gall, J. Köhler, The architecture and function of the light-harvesting apparatus of purple bacteria: from single molecules to in vivo membranes, Quart. Rev. Biophys., 39 (2006) 227-324.
[5] C.N. Hunter, Genetic manipulation of the antenna complexes of purple bacteria, in: R.E. Blakenship, M.T. Madigan, C.E. Bauer (Eds.) Anoxygenic Photosynthetic Bacteria, Kluwer Academic Publishers, Dordrecht, 1995, pp. 473-501.
[6] G. McDermott, S.M. Prince, A.A. Freer, A.M. Hawthornthwaite-Lawless, M.Z. Papiz, R.J. Cogdell, N.W. Isaacs, Crystal structure of an integral membrane light-harvesting complex from photosynthetic bacteria, Nature, 374 (1995) 517-521.
[7] S. Niwa, L.-J. Yu, K. Takeda, Y. Hirano, T. Kawakami, Z.-Y. Wang-Otomo, K. Miki, Structure of the LH1-RC complex from Thermochromatium tepidum at 3.0[thinsp]A, Nature, 508 (2014) 228-232.
[8] S. Bahatyrova, R.N. Frese, C.A. Siebert, J.D. Olsen, K.O. van der Werf, R. van Grondelle, R.A. Niederman, P.A. Bullough, C. Otto, C.N. Hunter, The native architecture of a photosynthetic membrane, Nature, 430 (2004) 1058-1062.
[9] J.D. Tucker, C.A. Siebert, M. Escalante, P.G. Adams, J.D. Olsen, C. Otto, D.L. Stokes, C.N. Hunter, Membrane invagination in Rhodobacter sphaeroides is initiated at curved regions of the cytoplasmic membrane, then forms both budded and fully detached spherical vesicles, Molecular Microbiology, 76 (2010) 833-847.
[10] M.L. Cartron, J.D. Olsen, M. Sener, P.J. Jackson, A.A. Brindley, P. Qian, M.J. Dickman, G.J. Leggett, K. Schulten, C. Neil Hunter, Integration of energy and electron transfer processes in the photosynthetic membrane of Rhodobacter sphaeroides, Biochimica et Biophysica Acta (BBA) - Bioenergetics, 1837 (2014) 1769-1780.
[11] M.R. Jones, Structural Plasticity of Reaction Centers from Purple Bacteria in: F.D. C. Neil Hunter, Marion C. Thurnauer, J. Thomas Beatty (Ed.) The Purple Phototrophic Bacteria, Springer, Dordrecht, The Netherlands, 2009, pp. 295-321.
[12] J. Deisenhofer, O. Epp, K. Miki, R. Huber, H. Michel, Structure of the protein subunits in the photosynthetic reaction centre of *Rhodopseudomonas viridis* at 3Å resolution, Nature, 318 (1985) 618-624.
[13] J.P. Allen, G. Feher, T.O. Yeates, H. Komiya, D.C. Rees, Structure of the reaction center from Rhodobacter sphaeroides R-26: the protein subunits, Proceedings of the National Academy of Sciences, 84 (1987) 6162-6166.
[14] S. Scheuring, J. Seguin, S. Marco, D. Lévy, B. Robert, J.-L. Rigaud, Nanodissection and high-resolution imaging of the Rhodopseudomonas viridis photosynthetic core complex in native membranes by AFM, Proceedings of the National Academy of Sciences, 100 (2003) 1690-1693.
[15] S. Scheuring, J.N. Sturgis, V. Prima, A. Bernadac, D. Lévy, J.-L. Rigaud, Watching the photosynthetic apparatus in native membranes, Proceedings of the National Academy of Sciences of the United States of America, 101 (2004) 11293-11297.

[16] S.J. Jamieson, P. Wang, P. Qian, J.Y. Kirkland, M.J. Conroy, C.N. Hunter, P.A. Bullough, Projection structure of the photosynthetic reaction centre–antenna complex of Rhodospirillum rubrum at 8.5 Å resolution, 2002.
[17] F. Francia, J. Wang, G. Venturoli, B.A. Melandri, W.P. Barz, D. Oesterhelt, The Reaction Center−LH1 Antenna Complex of Rhodobacter sphaeroides Contains One PufX Molecule Which Is Involved in Dimerization of This Complex, Biochemistry, 38 (1999) 6834-6845.
[18] A.W. Roszak, T.D. Howard, J. Southall, A.T. Gardiner, C.J. Law, N.W. Isaacs, R.J. Cogdell, Crystal structure of the RC-LH1 core complex from *Rhodopseudomonas palustris*, Science, 302 (2003) 1969-1972.
[19] F. Comayras, C. Jungas, J. Lavergne, Functional Consequences of the Organization of the Photosynthetic Apparatus in Rhodobacter sphaeroides: II. A STUDY OF PufX– MEMBRANES, Journal of Biological Chemistry, 280 (2005) 11214-11223.
[20] P.A. Bullough, P. Qian, C.N. Hunter, Reaction Center-Light-Harvesting Core Complexes of Purple Bacteria, in: F.D. C.N. Hunter, M.C. Thurnauer, J.T. Beatty (Ed.) The Purple Phototrophic Bacteria, Springer, Dordrecht, The Netherlands, 2009, pp. 155–179.
[21] P. Qian, P.A. Bullough, C.N. Hunter, Three-dimensional Reconstruction of a Membrane-bending Complex: The RC-LH1-Pu*f*x core dimer of Rhodobacter sphaeroides, Journal of Biological Chemistry, 283 (2008) 14002-14011.
[22] P. Qian, M.Z. Papiz, P.J. Jackson, A.A. Brindley, I.W. Ng, J.D. Olsen, M.J. Dickman, P.A. Bullough, C.N. Hunter, Three-Dimensional Structure of the Rhodobacter sphaeroides RC-LH1-PufX Complex: Dimerization and Quinone Channels Promoted by PufX, Biochemistry, 52 (2013) 7575-7585.
[23] P. Qian, C. Neil Hunter, P.A. Bullough, The 8.5 Å Projection Structure of the Core RC–LH1–PufX Dimer of Rhodobacter sphaeroides., Journal of Molecular Biology, 349 (2005) 948-960.
[24] J.N. Sturgis, J.D. Tucker, J.D. Olsen, C.N. Hunter, R.A. Niederman, Atomic Force Microscopy Studies of Native Photosynthetic Membranes, Biochemistry, 48 (2009) 3679-3698.
[25] R.N. Frese, C.A. Siebert, R.A. Niederman, C.N. Hunter, C. Otto, R. van Grondelle, The long-range organization of a native photosynthetic membrane, Proceedings of the National Academy of Sciences, 101 (2004) 17994-17999.
[26] P.G. Adams, D.J. Mothersole, I.W. Ng, J.D. Olsen, C.N. Hunter, Monomeric RC–LH1 core complexes retard LH2 assembly and intracytoplasmic membrane formation in PufX-minus mutants of Rhodobacter sphaeroides, Biochimica et Biophysica Acta (BBA) - Bioenergetics, 1807 (2011) 1044-1055.
[27] P.G. Adams, C.N. Hunter, Adaptation of intracytoplasmic membranes to altered light intensity in Rhodobacter sphaeroides, Biochimica et Biophysica Acta (BBA) - Bioenergetics, 1817 (2012) 1616-1627.
[28] E.C. Ratcliffe, R.B. Tunnicliffe, I.W. Ng, P.G. Adams, P. Qian, K. Holden-Dye, M.R. Jones, M.P. Williamson, C.N. Hunter, Experimental evidence that the membrane-spanning helix of PufX adopts a bent conformation that facilitates dimerisation of the Rhodobacter sphaeroides RC–LH1 complex through N-terminal interactions, Biochimica et Biophysica Acta (BBA) - Bioenergetics, 1807 (2011) 95-107.
[29] S. Scheuring, R.P. Gonçalves, V. Prima, J.N. Sturgis, The Photosynthetic Apparatus of Rhodopseudomonas palustris: Structures and Organization, Journal of Molecular Biology, 358 (2006) 83-96.
[30] L.-N. Liu, J.N. Sturgis, S. Scheuring, Native architecture of the photosynthetic membrane from Rhodobacter veldkampii, Journal of Structural Biology, 173 (2011) 138-145.
[31] K. Timpmann, M. Chenchiliyan, E. Jalviste, J.A. Timney, C.N. Hunter, A. Freiberg, Efficiency of light harvesting in a photosynthetic bacterium adapted to different levels of light, Biochimica et Biophysica Acta (BBA) - Bioenergetics, 1837 (2014) 1835-1846.
[32] B. Driscoll, C. Lunceford, S. Lin, K. Woronowicz, R.A. Niederman, N.W. Woodbury, Energy transfer properties of Rhodobacter sphaeroides chromatophores during adaptation to low light intensity, Physical Chemistry Chemical Physics, 16 (2014) 17133-17141.

[33] R.A. Niederman, D.E. Mallon, L.C. Parks, Membranes of Rhodopseudomonas sphaeroides. VI. Isolation of a fraction enriched in newly synthesized bacteriochlorophyll a-protein complexes, Biochim. Biophys. Acta, 555 (1979) 210-220.
[34] S.C. Chi, D.J. Mothersole, P. Dilbeck, D.M. Niedzwiedzki, H. Zhang, P. Qian, C. Vasilev, K.J. Grayson, P.J. Jackson, E.C. Martin, Y. Li, D. Holten, C. Neil Hunter, Assembly of functional photosystem complexes in Rhodobacter sphaeroides incorporating carotenoids from the spirilloxanthin pathway, Biochimica et Biophysica Acta (BBA) - Bioenergetics, 1847 (2015) 189-201.
[35] K. Holden-Dye, L.I. Crouch, M.R. Jones, Structure, function and interactions of the PufX protein, Biochimica et Biophysica Acta (BBA) - Bioenergetics, 1777 (2008) 613-630.
[36] M.R. Jones, G.J.S. Fowler, L.C.D. Gibson, G.G. Grief, J.D. Olsen, W. Crielaard, C.N. Hunter, Mutants of Rhodobacter sphaeroides lacking one or more pigment-protein complexes and complementation with reaction-center, LH1, and LH2 genes, Mol. Microbiol., 6 (1992) 1173-1184.
[37] A. Freiberg, P. Saari, Picosecond spectrochronography, IEEE J. Quantum Electron., QE-19 (1983) 622-630.
[38] A.Y. Borisov, A.M. Freiberg, V.I. Godik, K. Rebane, K. Timpmann, Kinetics of picosecond bacteriochlorophyll luminescence in vivo as a function of the reaction center state, Biochim. Biophys. Acta, 807 (1985) 221-229.
[39] J.P. Thornber, R.J. Cogdell, B.K. Pierson, R.E.B. Seftor, Pigment-protein complexes of purple photosynthetic bacteria: an overview, J. Cell. Biochem., 23 (1983) 159-169.
[40] R.J. Cogdell, H. Zuber, J.P. Thornber, G. Drews, G. Gingras, R.A. Niederman, W.W. Parson, G. Feher, Recommendations for the naming of photochemical reaction centers and light-harvesting pigment-protein complexes from purple photosynthetic bacteria, Biochim. Biophys. Acta, 806 (1985) 185-186.
[41] A. Freer, S. Prince, K. Sauer, M. Papiz, A. Hawthornthwaite-Lawless, G. McDermott, R. Cogdell, N.W. Isaacs, Pigment-pigment interactions and energy transfer in the antenna complex of the photosynthetic bacterium Rhodopseudomonas acidophila, Structure (London), 4 (1996) 449-462.
[42] M. Şener, J. Strümpfer, J.A. Timney, A. Freiberg, C.N. Hunter, K. Schulten, Photosynthetic Vesicle Architecture and Constraints on Efficient Energy Harvesting, Biophysical journal, 99 (2010) 67-75.
[43] R.J. Cogdell, R. Nechushtai, R. Malkin, Editors., Structure, Function and Biogenesis of Chlorophyll-Protein Complexes. [In: Photosynth. Res., 1995; 44(1-2)], Kluwer, Dordrecht, Neth., 1995.
[44] A. Freiberg, V.I. Godik, T. Pullerits, K.E. Timpmann, Directed picosecond excitation transport in purple photosynthetic bacteria, Chem. Phys., 128 (1988) 227-235.
[45] A.P. Shreve, J.K. Trautman, H.A. Frank, T.G. Owens, A.C. Albrecht, Femtosecond energy-transfer processes in the B800-850 light-harvesting complex of *Rhodobacter sphaeroides* 2.4.1, Biochim. Biophys. Acta, 1058 (1991) 280-288.
[46] A.M. Freiberg, V.I. Godik, S.G. Kharchenko, K. Timpmann, A.Y. Borisov, K. Rebane, Picosecond fluorescence of reaction centers from Rhodospirillum rubrum, FEBS Lett., 189 (1985) 341-344.
[47] H.W. Trissl, C.J. Law, R.J. Cogdell, Uphill energy transfer in LH2-containing purple bacteria at room temperature., Biochim. Biophys. Acta, 1412 (1999) 149-172.
[48] K.L. Zankel, R.K. Clayton, Uphill energy transfer in a photosynthetic bacterium, Photochemistry and Photobiology, 9 (1969) 7-15.
[49] T. Pullerits, A. Freiberg, Kinetic model of primary energy transfer and trapping in photosynthetic membranes, Biophys. J., 63 (1992) 879-896.
[50] T. Pullerits, K.J. Visscher, S. Hees, V. Sundstroem, A. Freiberg, K. Timpmann, R. van Grondelle, Energy transfer in the inhomogeneously broadened core antenna of purple bacteria: a simultaneous fit of low-intensity picosecond absorption and fluorescence kinetics, Biophys. J., 66 (1994) 236-248.
[51] L. Valkunas, V. Liuolia, A. Freiberg, Picosecond processes in chromatophores at various excitation intensities, Photosynth. Res., 27 (1991) 83-95.

[52] J.G.C. Bakker, R. Van Grondelle, W.T.F. Den Hollander, Trapping, loss and annihilation of excitations in a photosynthetic system. II. Experiments with the purple bacteria Rhodospirillum rubrum and Rhodopseudomonas capsulata, Biochim. Biophys. Acta, 725 (1983) 508-518.
[53] G. Paillotin, N.E. Geacintov, J. Breton, A master equation theory of fluorescence induction, photochemical yield, and singlet-triplet exciton quenching in photosynthetic systems, Biophys. J., 44 (1983) 65-77.
[54] A. Freiberg, V.I. Godik, T. Pullerits, K. Timpman, Picosecond dynamics of directed excitation transfer in spectrally heterogeneous light-harvesting antenna of purple bacteria, Biochim. Biophys. Acta, 973 (1989) 93-104.
[55] R. Van Grondelle, Excitation energy transfer, trapping and annihilation in photosynthetic systems, Biochim. Biophys. Acta, 811 (1985) 147-195.
[56] R.K. Clayton, S.C. Straley, Photochemical electron transport in photosynthetic reaction centers. IV. Observations related to the reduced photoproducts, Biophys. J., 12 (1972) 1221-1234.
[57] K. Timpmann, F.G. Zhang, A. Freiberg, V. Sundström, Detrapping of excitation energy from the reaction center in the photosynthetic purple bacterium *Rhodospirillum rubrum*, Biochim. Biophys. Acta, 1183 (1993) 185-193.
[58] K. Timpmann, A. Freiberg, V. Sundström, Energy trapping and detrapping in the photosynthetic bacterium *Rhodopseudomonas viridis*: transfer-to-trap-limited dynamics, Chem. Phys., 194 (1995) 275-283.
[59] A. Freiberg, J.P. Allen, J. Williams, N.W. Woodbury, Energy trapping and detrapping by wild type and mutant reaction centers of purple non-sulfur bacteria, Photosynth. Res., 48 (1996) 309-319.
[60] O.J.G. Somsen, L. Valkunas, R. van Grondelle, A perturbed two-level model for exciton trapping in small photosynthetic systems, Biophys. J., 70 (1996) 669-683.
[61] C.N. Hunter, R. Van Grondelle, N.G. Holmes, O.T.G. Jones, R.A. Niederman, Fluorescence yield properties of a fraction enriched in newly synthesized bacteriochlorophyll a-protein complexes from Rhodopseudomonas sphaeroides, Photochem. Photobiol., 30 (1979) 313-316.
[62] F. Comayras, C. Jungas, J. Lavergne, Functional Consequences of the Organization of the Photosynthetic Apparatus in Rhodobacter sphaeroides: I. Quinone domains and excitation transfer in chromatophores and reaction center center.antenna complexes., Journal of Biological Chemistry, 280 (2005) 11203-11213.
[63] M. Şener, J. Hsin, L.G. Trabuco, E. Villa, P. Qian, C.N. Hunter, K. Schulten, Structural model and excitonic properties of the dimeric RC–LH1–PufX complex from Rhodobacter sphaeroides, Chemical Physics, 357 (2009) 188-197.
[64] J. Hsin, J. Strümpfer, M. Şener, P. Qian, C.N. Hunter, K. Schulten, Energy transfer dynamics in an RC–LH1–PufX tubular photosynthetic membrane, New Journal of Physics, 12 (2010) 085005.
[65] M.K. Şener, J.D. Olsen, C.N. Hunter, K. Schulten, Atomic-level structural and functional model of a bacterial photosynthetic membrane vesicle, Proceedings of the National Academy of Sciences, 104 (2007) 15723-15728.
[66] M. Şener, J. Strümpfer, J. Hsin, D. Chandler, S. Scheuring, C.N. Hunter, K. Schulten, Förster Energy Transfer Theory as Reflected in the Structures of Photosynthetic Light-Harvesting Systems, ChemPhysChem, 12 (2011) 518-531.

Figure captions

Figure 1. (A, B) Comparison of the absorption spectra of membranes from Rba. sphaeroides strains containing monomeric (red) or dimeric (blue) core complexes, and with low (A, C, E) or high (B, D, F) content of LH2. The red arrows indicate the selective excitations used in stationary fluorescence measurements described in section 3.2. (C-F) Decomposition of the spectra for the same samples. The sub-spectra of the LH2-only and D-only membranes used in the fit are coloured in green and black, respectively. The measured curves are shown in red (monomeric) or blue (dimeric) and the simulated curves in grey. Each inset in panels C-F illustrates the composition of samples. Two (one) red rings indicate high (low) relative LH2

content, respectively, each green dot represents the bacteriochlorophyll-a (BChl) αβ-$BChl_2$ heterodimer subunit of the LH1 core complex, a light yellow dot represents PufX polypeptide and a blue circle represents RC.

Fig. 2. Normalized fluorescence spectra of the samples with dimeric or monomeric LH1 core and with high (A, C) or low (B, D) LH2 content following excitation at 800 nm (A, B) or at 915 nm (C, D). The samples with dimeric core are shown by blue curves and those with monomeric core, by red curves. All the spectra are measured at saturated state of photosynthesis. The inset of panel A shows the deconvolution of the DH fluorescence spectrum (blue) at 800-nm excitation into the F850 (green curve) and F875 (black curve) constituents. The component spectra used in the fit are measured spectra of LH2-only sample and D-only sample. The sum of the components (narrow magenta line) is practically overlapping with the measured spectrum. The red arrow highlights the extra LH2 fluorescence emission observed in the ML sample. A scattered excitation light artefact in panels C and D is evident at 915 nm. Hatched area in panel B indicates the spectral range of the band pass filter used in the intensity dependent kinetic measurements (Section 3.3).

Figure 3. Dependence of the fluorescence yield, F850/F875, on the LH2 to RC ratio upon 800 nm (squares) and 915 nm (rhombi) excitations. The data for dimeric and monomeric core samples are distinguished by blue and red colours, respectively. The lines connecting these data points are for guiding the eye. The correspondingly coloured dashed lines with un-filled data points display the calculated fluorescence yield ratios, as described in Section 4.1. The dashed rectangular outlines the data point most drastically deviating from modelling result. The data at LH2/RC = 0 correspond to the samples comprising solely core complexes.

Figure 4. Excitation intensity dependence of the dominant short fluorescence lifetime component (filled spheres, left Y-axis) and the fluorescence yield (open circles, right Y-axis). The data for dimeric and monomeric core samples are distinguished by blue and red colours, respectively. Panels A and B, correspondingly, present data of high and low LH2 content samples. The yield data are scaled until matching with lifetime values in order to visualize the proportionality of these quantities. The increase in lifetime and yield corresponds to the transition from the open to the closed RC state. The samples from Rba. sphaeroides were excited at 590 nm for the decay kinetics and at 800 nm for the stationary fluorescence yield measurements.

Figure 5. Kinetic scheme of exciton population dynamics of the photosynthetic unit of purple bacteria. The basic scheme (right from the vertical dotted demarcation line) comprises functionally connected LH2 and LH1 compartments. An additional compartment used in the extended model represents functionally unconnected or poorly connected LH2 pool. The total absorbed power is denoted by P. Red arrows illustrate the branching of the absorbed power between the compartments governed by the factors j and x, where $0 \leq j,x \leq 1$. The factor x represents a fraction of unconnected LH2 units. Each kinetic pathway is characterized by a rate constant.

Fig. 6. The dependence of quantum efficiency of active photosynthesis on the LH2 to RC ratio in dimeric (A) and monomeric (B) core samples upon 800 (squares) and 915 nm (rhombi) excitation. The open data points at LH2/RC=0 correspond to the quantum efficiencies of the imaginary membranes containing either sole dimeric or sole monomeric core complexes. The shaded area features the ~2% estimated standard deviation in the efficiency. The lines represent linear fits of the data points. See text for further explanations.

Table captions

Table 2. Composition of the samples tested in the current study.

Table 2. Ratio of the LH2 to RC complexes (±5%) in Rba. sphaeroides strains with LH2 and core monomers or dimers.

Table 3. The dominant short fluorescence lifetime component (±10%) in picoseconds corresponding to active (noted by superscript o) and saturated (superscript c) ranges of photosynthesis with, respectively, mostly open and mostly closed RCs.

Table 4. The lifetime in picoseconds of the dominant short component of the fluorescence decay (±10%) at blue and red ends of the fluorescence spectrum in case of active and saturated photosynthesis.

Table 5. The calculated microscopic forward energy transfer time, ${k_1}^{-1}$, backward energy transfer time, ${k_{-1}}^{-1}$, quenching time either by open RC, ${k_2}^{o^{-1}}$, or by closed RC, ${k_2}^{c^{-1}}$, apparent LH2->LH1energy transfer time in case of open (closed) RC, $\gamma_1^{o^{-1}}$ ($\gamma_1^{c^{-1}}$), and apparent trapping time, $\gamma_2^{o^{-1}}$, and apparent quenching time, $\gamma_2^{c^{-1}}$**.** All the calculated times have an uncertainty up to 10% of their numerical value.